Numerical simulation of hydrodynamic cavitation in acetic acid solutions with different concentrations

Numerical simulation of hydrodynamic cavitation in acetic acid solutions with different concentrations

Lili Zhang [1,3], Ning Mao [1], Can Kang [1,2] and Ziwen Zou[1]

[1] School of Energy and Power Engineering, Jiangsu University, Zhenjiang 212013, China;
[2] Key Laboratory of China Machinery Industry for Centrifugal Pumps, Zhenjiang 212013, China.

[3] Email: m18852899906@163.com

Abstract. To investigate cavitation phenomenon in acetic acid solution, numerical simulation was performed using the commercial computational fluid dynamics code of ANSYS Fluent. A comparison for acetic acid solutions of different concentrations flowing in a Venturi tube was implemented, focusing on the effect of the solution concentration on cavitation. Distributions of velocity, static pressure as well as the volume fraction of cavitation in the Venturi tube were analyzed. Flow and cavitation characteristics were explained. The results show that the non-uniformity of pressure distribution is enhanced with the increase of the solution concentration. Cavitation in the Venturi tube is featured by cavitation clouds. As the solution concentration rises, the length of the cavitation cloud decreases, and the cavitation intensity decays continuously. The results of this study can contribute to raise the effectivity and environmental efficiency of cleaning applications of acetic acid solutions.

1. Introduction

Acid solutions have been used to clean rusted or contaminated surface. Nevertheless, improperly selected concentration of acid solutions might cause hydrogen embrittlement of metal materials and corrosion of the target surface. Meanwhile, residual acid endangers the environment [1]. As the acid solution is used together with cavitation, effective cleaning effect is expected even at low solution concentration. In this context, hydrodynamic cavitation is a suitable strategy. Venturi tubes have been used as cavitation reactors [2]. Nevertheless, most of the literature employed pure water as the liquid medium to nurture cavitation. Both experimental and numerical works were documented. Moreover, the applications cover a wide range from pulping process to environmental engineering [3].

The present study lays emphasis on hydrodynamic cavitation of acetic acid solutions in the Venturi tube. Two solution concentrations of 5% and 10% were considered. In view of the corrosive effect of acetic acid solutions on plexiglass, experimental observation of the cavitation is impractical. Therefore, computational fluid dynamics (CFD) technique was used. The commercial CFD code of ANSYS Fluent was used to solve flow and cavitation equations [4]. Distributions of flow quantities in the Venturi tube were obtained. Furthermore, distributions of cavitation volume fraction were described and compared. The conclusions shed light on the effect of liquid medium on hydrodynamic cavitation and supplement the knowledge of cavitation phenomenon.

2. Experimental device

An experimental loop was built to visualize cavitation in the Venturi tube with medium of pure water, as shown in Figure 1. The pipe diameter is 50 mm, the operating temperature is 293.15K,the volume of liquid is 0.68 m^3 . Furthermore, the experimental observation was used to validate the numerical scheme. The image of the Venturi tube used in experiments is exhibited in Figure 2. Both the inlet and outlet diameters of the Venturi tube are 50 mm. Both the diameter and length of the throat segment are 20 mm. The lengths of the convergent and divergent segments are 80 and 200 mm, respectively. The adopted geometry was based on generally accepted standards for cavitation reactors in the form of Venturi tubes [5].

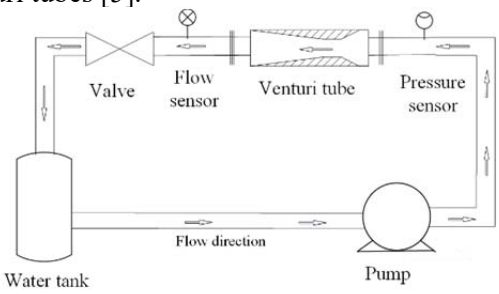

Figure 1. Schematic view of the loop for visualizing cavitation in the Venturi tube.

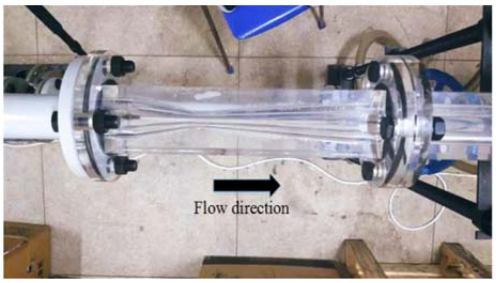

Figure 2. Image of the Venturi tube used in the experiment.

3. Numerical simulation

3.1. Governing equations and simulation models

Here, the three liquid mediums in the Venturi tube, pure water, 5% and 10% acetic acid solutions were regarded as incompressible Newtonian fluids [6]. Flows conformed to Reynolds average N-S (RANS) equations. The RNG $k-\varepsilon$ turbulence model was used in the simulation. The Schnerr-Sauer model [7] was selected for describing the inception and development of cavitation.

3.2. Boundary conditions

The total pressure inlet boundary condition was set at the inlet of the computational domain and the value of the total pressure was 105,525 Pa. According to the experimental data, the static pressure outlet boundary condition was set at the domain outlet with the pressure of 75,525 Pa. The operating pressure was set to 0 atm. No-slip boundary conditions were set for all fluid-wetted walls. Physical properties of the three liquid mediums are listed in Table 1. As temperature remains constant, the saturated vapor pressure varies with the solution concentration. According to Raoult's law, the saturated vapor pressure can be calculated through its dependence on the solution concentration. In the Venturi tube, different concentrations of acetic acid solutions entail different flow patterns and the positions where cavitation occurs. To compare various cavitation phenomena associated with different solution concentrations, the cavitation number proposed in the previous work was adopted [8]. For the cavitation simulation, the initial diameter of cavitation nuclei was set to be 1×10^{-5} m. The initial mass fraction of cavitation was assumed to be 1.5×10^{-5}.

Table 1. Physical properties of acetic acid solutions.

Liquid medium	Density (kg/m3)	Dynamic viscosity (mPa·s)	Vapor pressure (Pa)
Pure water	998.2	1.003	2333
5% Acetic acid solution	1005.5	1.095	2296
10% Acetic acid solution	1012.5	1.22	2257

To discretize spatially the computational domain, the commercial code of ICEM CFD was used to generate meshes. Structural meshes were used to improve the simulation accuracy. Meanwhile, meshes near the medium-wetted walls were refined to capture flow phenomena caused by high velocity gradients. After a mesh independence examination, the total number of meshes of 2,004,750 was used in subsequent simulations, and the total node number is 2038700. The y+ values range between 30 and 70.

4. Results analysis

4.1. Comparison of numerical and experimental results

A comparison of experimental and numerical results is illustrated in Figure 3, where pure water was flowing in the Venturi tube with the volumetric flow rate of 20 m^3/h. It is seen that cavities develop from the throat to the divergent segment, which is shared by the two cases. In particular, the cavity lengths in streamwise direction are nearly equivalent for the two cases. In this context, numerically obtained cavity profiles are relatively smooth. This is reasonable in consideration of the surface roughness that cannot be modelled in simulation. The cavitation volume fraction obtained numerically is 2.84×10^{-2}, and the corresponding experimental result is 2.79×10^{-2}. The difference between them is acceptable. Overall, the numerical scheme is reliable.

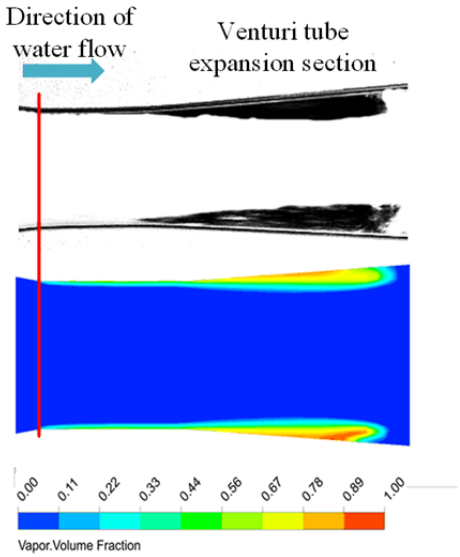

Figure 3. Comparison of experimentally and numerically obtained cavity profiles.

4.2. Static pressure distribution

Static pressure distributions in the Venturi tube are shown in Figure 4. To extract quantitative information, a comparison of pressure distributions over the tube axis for the three liquids is illustrated in Figure 5. In Figure 4, the volumetric flow rates of the three liquids are identically 20 m^3/h. It is seen that static pressure varies gradually but not monotonously from the tube inlet to the outlet. The variation trends for the three cases are similar. Static pressure in the divergent section of the Venturi tube is still lower than the initial pressure, which is related to the collapse of the cavitation bubbles in the divergent section and the loss caused by resistance. It is seen in Figure 5 that in the divergent segment of the Venturi tube, the slope of the static pressure distribution curve associated with10% acetic acid solution is relatively larger. Therefore, static pressure varies quickly. It is identifiable that the uniformity of static pressure distribution decays with the increase of the solution concentration.

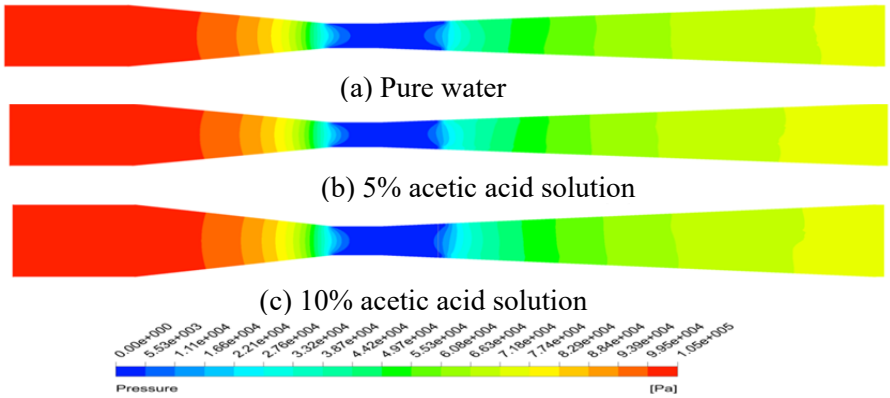

Figure 4. Statistic pressure distributions in the Venturi tube.

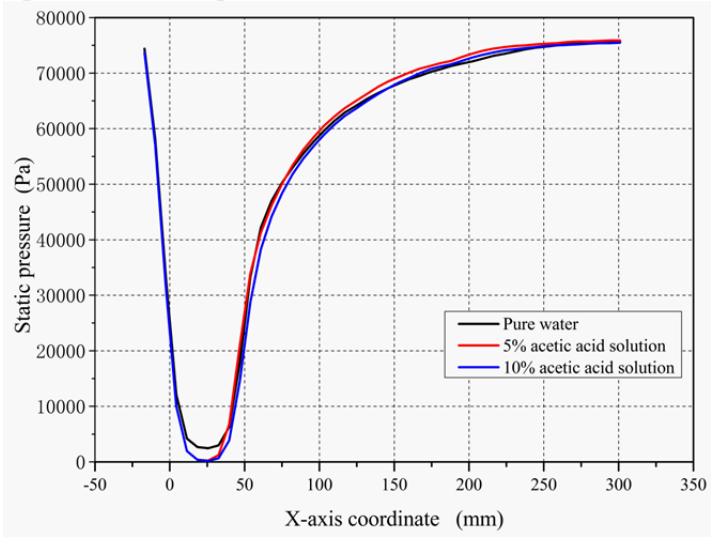

Figure 5. Distributions of static pressure over the Venturi tube axis for of the three liquids.

4.3. Turbulent viscosity

Distributions of turbulent viscosity at the volumetric flow rate of 20 m^3/h are shown in Figure 6. It is seen that the turbulent viscosity distributions of the three liquids are different and overall turbulent viscosity of 10% acetic acid solution is the highest.

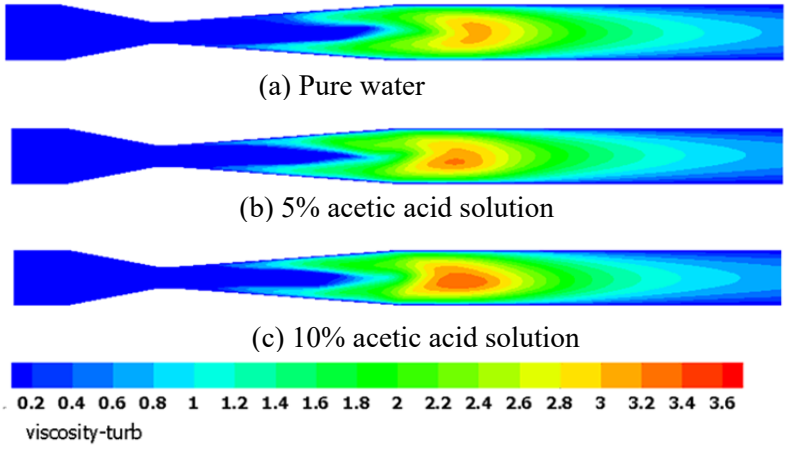

Figure 6. Distributions of turbulent viscosity in the Venturi tube.

The solution with high viscosity suffers from high resistance in the divergent segment, thus reducing the flow velocity. The viscosity of the acetic acid solution increases with the solution concentration; therefore, 10% acetic acid solution is responsible for the lowest overall velocity in the divergent segment.

4.4. Distribution of cavitation volume fraction

Distributions of cavitation volume fraction are shown in Figure 7. The shape of the cavitation cloud exhibited in Figure 7 is in accordance with that documented in [9]. The cavity length reduces with the increase in the solution concentration. The cavitation volume fractions of pure water, 5% and 10% acetic acid solutions are 2.84×10^{-2}, 2.39×10^{-2}, and 2.316×10^{-2}, respectively. As liquid viscosity ascends, the ambient liquid resistance is enhanced. Therefore, the cavity length is minimized with the increase in the solution concentration.

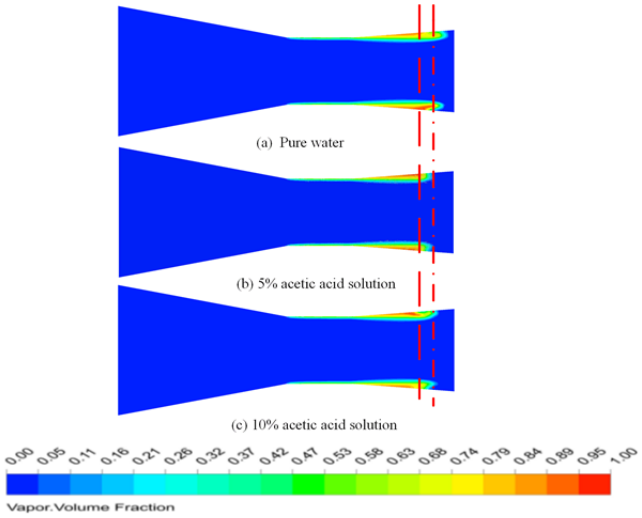

Figure 7. Distributions of cavitation volume fraction.

With Figure 7, it is difficult to obtain a full view of the cavity cloud. Here, four cross sections of the divergent part of the Venturi tube, Cross sections A, B, C and D, which were deployed respectively with the streamwise distance of 10, 15, 20, and 25 mm from the outlet of the throat segment were monitored. It is observed that cavitation collapses completely at Cross section D. Distributions of cavitation volume fraction over Cross sections A, B and C are shown in Figures 8, 9 and 10. The three figures share apparent similarity. On Cross section A, the distribution of cavitation volume fraction is regular and the maximum cavitation volume fraction arises at the tube wall. Meanwhile, in circumferential direction, the distribution is uniform. From Cross sections B to C, the asymmetry of the distribution of the cavitation volume fraction is undermined. The development of cavitation is hindered by elevated static pressure.

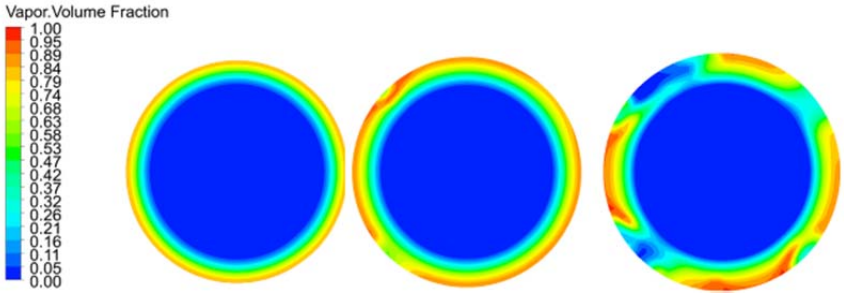

(a) Cross section A (b) Cross section B (c) Cross section C

Figure 8. Cross-sectional distribution of cavitation volume fraction for pure water.

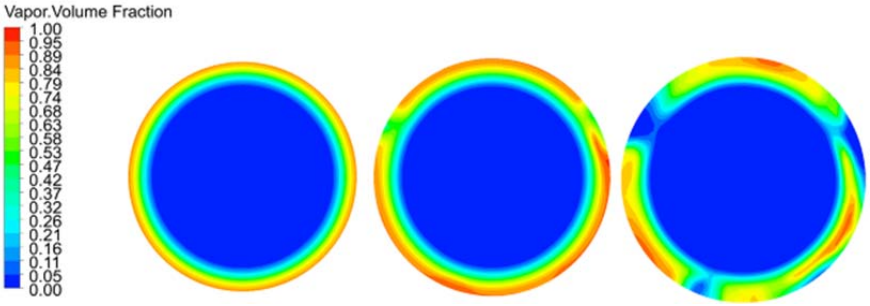

(a) Cross section A (b) Cross section B (c) Cross section C

Figure 9. Cross-sectional distribution of cavitation volume fraction for 5% acetic acid solution.

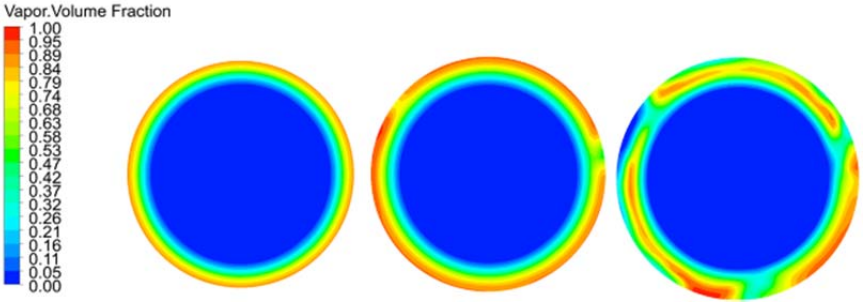

(a) Cross section A (b) Cross section B (c) Cross section C

Figure 10. Cross-sectional distribution of cavitation volume fraction for 10% acetic acid solution.

4.5. Relationship between cavitation number and the solution concentration

To evaluate the cavitation intensity among the four cross sections considered, cavitation number was calculated based on the static pressure averaged over each cross section. The results are plotted in Figure 11. Large cavitation number corresponds to low cavitation intensity. In Figure 11, as the distance from the throat segment grows, cavitation number decreases firstly and then increases continuously. The smallest cavitation number in the two acetic acid solutions appears closer to the throat than in the case of pure water. This demonstrates that the contribution of pressure recovery on the suppression of cavitation cannot take effect immediately. It is seen in Figure 11 that cavitation number of pure water is smaller than its counterparts. Therefore, cavitation effect in the Venturi tube is the strongest as pure water is used instead of the two acetic acid solutions.

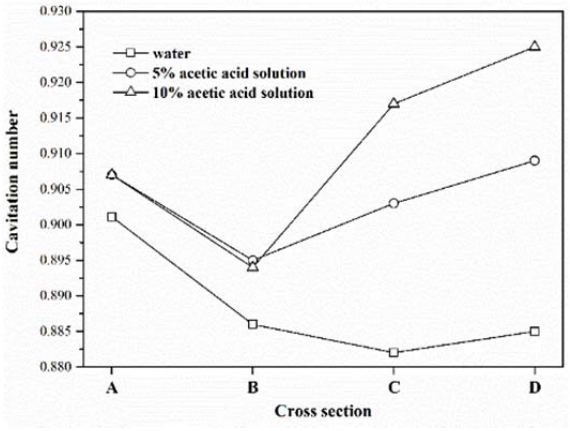

Figure 11. Variation of cavitation number over four cross sections.

5. Conclusions

Acetic acid solutions with different concentrations flowing through the Venturi tube were numerically investigated. With the increase of the solution concentration, the non-uniformity of static pressure distributions is enhanced and overall velocity declines.

The solution concentration of the acetic acid solution imposes a significant effect on hydrodynamic cavitation. The increase of the solution concentration entails the reduction of the Reynolds number. The length of the cavitation cloud in the Venturi tube decreases

With the progression of cavities from the throat to the divergent segment, cavities tend to be disintegrated, which occurs earlier in acetic acid solutions. As the concentration of acetic acid solution increases, cavitation number increases and the cavitation intensity decays.

References

[1] Román M F S, Gándara I O, Ibañez R, et al 2012 *J. Membrane. Sci* **415** 616
[2] Albanese L, Ciriminna R, Meneguzzo F, et al 2017 *J.Clean.Prod* **142** 1457
[3] Shankar,V, Lundberg,A,Frenander,A, 2018 *J.Fluid Flow Heat Mass Transfer* **5**
[4] Jangir N, Diwedi P, Ghosh S. 2017 *Chem.Eng.Process* **122**
[5] Sun Y, Niu W 2012 *Modell. Simul. Eng* **12**
[6] Zhang J X 2017 *AIP Adv* **7** 99
[7] Zhu J, Chen Y, Zhao D, et al 2015 *Eur J Mesh B-Fluid* **52**
[8] Brinkhorst S, Lavante E V 2017 *Flow Meas. Instrum* **54** 56
[9] Long X, Zhang J, Wang J, et al 2017 *Int. J. Multiphas Flow* **89** 290